Comprehensive Electrochemical-Chemical Study of Copper Reduction from Molybdenum Concentrate Using Mixed HCl, FeCl$_3$, CuCl$_2$, and CaCl$_2$ Leaching Medium

Shima Barakan[1] · Valeh Aghazadeh[1] · Ehsan Bidari[1,2] · Mina Soleymani[1] · Morovvat Faridazad[1]

Abstract

Molybdenite is the most important molybdenum concentrate, which is mainly recovered as a by-product from porphyry copper deposits. Due to the low efficiency of purification processes such as flotation in the reduction of copper content of molybdenum concentrate to a standard level (i.e., less than 0.5 wt.%), further purification by a hydrometallurgical method is required. Although different types of chemical reagents were found to be effective in the leaching of copper minerals from molybdenum concentrate, the mechanisms of these processes remain largely unexplored. In this study, optimal conditions for maximum copper leaching (> 99%) were obtained at the concentration of HCl = 1 M, FeCl$_3$ = 0.5 M, CuCl$_2$ = 0.05 M, CaCl$_2$ = 0.5 M at 75 °C, 500 rpm, and S:L = 1:10 during 60 min. CuCl$_2$ was identified as the most effective leaching reagent for copper dissolution in agreement with Visual MINTEQ model results due to the formation of various types of copper chloride complexes. Furthermore, the electrochemical behaviors of FeCl$_3$, CuCl$_2$, and CaCl$_2$ reagents before and after the leaching process were investigated by the cyclic voltammetry technique. The results of cyclic voltammograms at different scan rates verified the presence of copper chloride complexes, and ferric ions as the oxidizing reagents for better dissolution of copper sulfides. Based on kinetic study results of shrinking core models, both chemical and diffusion reactions controlled the copper leaching process with an obtained activation energy of 33.56 kJ/mol. For recovery of the leached copper, the precipitation process was done by the addition of Na$_2$S at 45 °C, S/Cu = 1, and pH = 9.

Keywords Copper dissolution · Molybdenite · Oxidizing reagent · Copper leaching kinetics

1 Introduction

Molybdenum plays an important role in the energy industry and green technologies in resistant steel, cracking agents, the oil and gas industry, cast iron, and catalysts [44]. The decrease of high-grade molybdenum resources has received much attention in the processing of low-grade ore deposits of this mineral [24]. Molybdenum can be obtained directly or as a by-product of processing in copper mines. Porphyry copper deposits contain molybdenum in the form of molybdenite (MoS$_2$) [1]. In these sulfide minerals, a bulk

copper-molybdenum concentrate is formed, and the reduction of the copper amount is necessary for molybdenum separation [38].

Many metallurgical methods, such as smelting, roasting [22], direct reduction of molybdenite [31], and plasma smelting [47], have been used in the production of molybdenum. Chlorination methods are another common method for the purification and separation of molybdenum [37]. The disadvantages of pyrometallurgical processes are several processing steps, problems in reducing the trioxide to metal, low recoveries, and SO$_2$ pollution [24]. According to industrial demand and environmental protection rules, the selection of non-toxic, efficient, and low-cost methods for refractory sulfide concentrate is necessary. In this way, the hydrometallurgical processes have become attractive due to their low-energy consumption, no emission of SO$_2$, and they could be applicable for low-grade deposits to achieve highly purified molybdenum [50].

✉ Valeh Aghazadeh
v.aghazadeh@sut.ac.ir

1 Department of Mineral Processing, Faculty of Mining Engineering, Sahand University of Technology, Tabriz, Iran

2 TU Bergakademie Freiberg, Institute of Inorganic Chemistry, Leipziger, Freiberg, Germany

The conventional method for molybdenum purification is flotation [30, 51]. However, this method is not highly efficient in the effective reduction of copper amounts in the economic range of less than 0.5% Cu. The concentrates produced by flotation often contain 1.0–1.5% Cu, and further chemical purification processing for the removal of Cu is largely required [19, 41]. The application of hydrometallurgical methods such as solvent extraction (SX) [14], ion exchange [12], using sodium hypochlorite agent [53], leaching of sulfidized iron copper sulfide [36, 45], electrooxidation method [43], bioleaching [40], pressure oxidative leaching [11], alkali leaching, and acidic leaching (e.g., ferric sulfate, ferric chloride leaching, sulfuric acid leaching (H_2SO_4), hydrochloric acid (HCl), nitric acid leaching (HNO_3), and cyanide leaching processes) have been used for copper removal from molybdenum concentrates [39].

Since 1970, molybdenite leaching has been frequently used for copper removal [5]. The application of leaching processes for molybdenite separation and purification from porphyry copper deposits represented slow leaching kinetics because of the presence of primary sulfide minerals such as chalcopyrite ($CuFeS_2$) in comparison with the secondary copper sulfides such as covellite (CuS) and chalcocite (Cu_2S) [15]. The formation of a passive layer (e.g., elemental sulfur, polysulfide, jarosite, and ferric oxyhydroxide) is the other issue to prevent copper dissolution from molybdenite [46]. Therefore, to improve the dissolution of chalcopyrite from molybdenite, HCl acid leaching has been used under oxidative conditions. In this area, oxidizing agents such as cupric chloride ($CuCl_2$) and ferric chloride ($FeCl_3$) could be effective for better dissolution of refractory copper sulfides [2]. Based on previous studies, one of the advantages of using ferric chloride in an acidic medium with HCl is the possibility of reproducing ferric ions from ferrous ions. Moreover, the presence of chloride ions in the acidic leaching could be an effective way to prevent the passivation and the formation of porous sulfur structures [29]. In acidic media, using cupric chloride also plays an important role in increasing copper leaching by the formation of various chloride complexes (e.g., Cu^+, $CuCl^+$, $CuCl_2^-$, $CuCl_3^-$, $CuCl_4^-$) on the external surface of chalcopyrite [49]. Moreover, cupric chloride showed a synergistic effect on the dissolution reaction of chalcopyrite in ferric chloride [28].

This research is devoted to the important problem of the increase in the quantity of pure molybdenite. One of the main objectives of this research was to determine the optimum conditions for copper removal from molybdenite concentrates without creating a passive layer that prevents copper dissolution. This study is a part of the research carried out at Sungun copper mine plant located in East Azerbaijan province, northwest of Iran. In Sungun copper mine, a flotation method was used for the floating of molybdenite and copper sulfide minerals (i.e., with depression of pyrite).

After that, in the molybdenum plant, the purification methods were carried out for the selective separation of molybdenite. Whereas the copper minerals in Sungun copper mine are located at high depths related to chalcopyrite, in this flotation method, the consumption of sodium sulfide (i.e., used as an inorganic depressant) has excessively resulted in environmental problems without efficient molybdenite separation. On the other hand, the copper amount was increased due to the presence of chalcopyrite in the molybdenum concentrate and it was not at the standard level (i.e., more than 0.5% Cu). Thus, based on mineralogical/chemical compositions of molybdenite, and facilities for implementing hydrometallurgy processing units, initial laboratory experiments were designed and applied. Due to the lack of comprehensive evaluation of acidic leaching conditions for copper dissolution from molybdenum concentrates, this study simulated the leaching conditions.

The dissolution of chalcopyrite is also dependent on potential and electrochemical reactions. In some studies, the relationship between the solution potential and the leaching rate has been investigated to solve the difficulty of chalcopyrite leaching [48]. This research brings a new perspective into focus on the cyclic voltammetry technique to determine the electrochemical behavior of leaching agents for copper removal from chalcopyrite existed in molybdenum concentrate. For a better understanding of electrochemical reactions and reaction mechanisms, cyclic voltammetry was used to study the qualitative and quantitative electrochemical properties of electroactive species in leaching solution. In addition, to obtain the leached copper from the leaching solution, the precipitation of copper was carried out under different conditions. The present research was conducted by kinetics, chemical equilibrium modeling, and redox potential of the solution to identify the optimum conditions and effective reagents for copper dissolution without any changing phase of molybdenite in the hope of up-scaling this leaching process in the Sungun copper mine plant and the other mining plants with similar conditions.

2 Materials and Methods

2.1 Materials

The molybdenum concentrate used in this study was obtained from the copper-molybdenum processing complex of Sungun mine, East Azerbaijan province, Iran. Chemical reagents used for preparing leaching solutions consisted of HCl (37% v/v), $FeCl_3$ (98–99 wt.%), and $CaCl_2 \cdot 2H_2O$ (98–99 wt.%) was obtained from the Chemistry Center of Iran Co. Moreover, $CuCl_2 \cdot 2H2O$ reagent was prepared (98–99% wt.) by Dr. Mojallali Co. In the precipitation

process, $Ca(OH)_2$ (98–99 wt.%) and Na_2S (98–99 wt.%) were obtained from Merck Co and Dr. Mojallali Co.

2.2 Experimental Procedures

Leaching tests were performed in a 1-L glass reactor with a water-cooled condenser and water bath equipment, as shown in Fig. 1. For each test, after adjusting the desired

Fig. 1 Schematic diagram of copper dissolution and copper precipitation processes

temperature, 500 cm^3 of a leaching solution was added to the reactor. After adding the molybdenite sample, the reactor was sealed (i.e., there were three holes for keeping a thermometer, a redox electrode, and collecting samples). The solution was agitated at various agitation speeds with a teflon impeller during the leaching test. During the leaching process, several samples were collected to analyze the copper (Cu) concentrations. After investigating the leaching conditions, the optimum concentrations of each leaching agent, contact time, S:L ratio, stirring speed, and temperature were obtained.

To precipitate copper from the leaching solution, and to prevent H_2S formation, pH > 7 was maintained. After adjusting pH, sodium sulfide was added at different S/Cu ratios and temperatures. At designated times, some samples were withdrawn to analyze the copper concentration. Table 1 shows the experimental conditions for the molybdenite leaching and copper precipitation processes. The steps of the copper dissolution processes and copper precipitation are shown in Fig. 1.
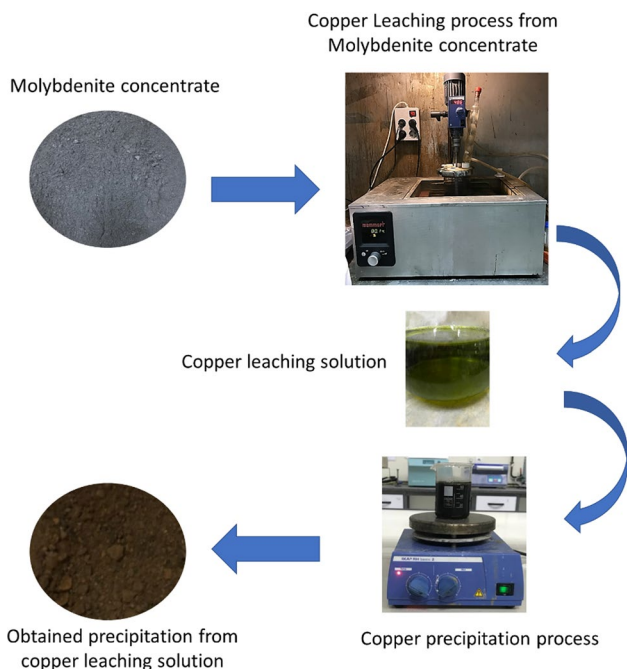
2.3 Methods of Characterization

Laser particle size distribution analysis (LPSA, Analysette 22 NanoTec device) was used to measure the particle size fraction of molybdenum concentrate. To analyze the chemical composition of the molybdenum concentrate, inductively coupled plasma atomic emission spectroscopy (ICP-OES, ES-730) was used by the peroxide fusion preparation method. The concentrations of inorganic elements in the leachate solution were also measured by ICP-OES, Varian 730-ES with HF-Multi Acid Digest. The X-ray powder diffraction (XRD) data were recorded

Table 1 Copper leaching from molybdenum concentrate and copper precipitation process conditions

Laching process for copper dissolution						
Effective parameters	Conditions					
HCl conc. (M)	0.5	1	2	3	-	-
FeCl$_3$ conc. (M)	0	0.2	0.5	0.7	1	-
CuCl$_2$ conc. (M)	0	0.01	0.05	0.1	-	-
CaCl$_2$ conc. (M)	0	0.5	1	3	-	-
S:L ratio	1:20	1:10	1:5	-	-	-
Temperature (°C)	25	35	55	75	95	-
Stirring speed (rpm)	300	500	700	-	-	-
Leaching time (min)	5	15	30	60	180	240
Copper precipitation process						
Effective parameters	Conditions					
pH	8	9	10	-	-	-
S:Cu ratio	0.5	1	1.5	-	-	-
Temperature (°C)	25	45	65	-	-	-
Contact time (min)	1	5	15	30	-	-

by Expert Pro-PHILIPS Co., diffractometer using Cu Kα radiation in the $2\theta = 2$–$80°$ with step time = 0.03 s and step size $2\theta = 0.02°$. To identify the mineralogical phase of each sample, the XRD pattern was analyzed by X'Pert High Score Plus software. Atomic absorption spectroscopy (AAS-novAA300) was used for the determination of copper concentration before/after leaching and precipitation processes. For the mineralogy study of molybdenum concentrate and to find the interlocking between molybdenite and copper sulfide minerals, optical microscopy on some polished sections of molybdenum concentrate was carried out by a polarizing optical microscope (SM-LUX-POL). Field emission scanning electron microscopy and energy dispersive spectrometer (FESEM-EDS) were also used to characterize the morphology and semi-quantitative analysis of molybdenite. An oxygen reduction potential (ORP) electrode was incorporated with a Pt electrode into a KCl-saturated Ag/AgCl reference electrode and inserted into the leaching solution to measure the total potential for the leaching process. The Laboratory pH meter 827 Metrohm equipped with a glass pH-responsive electrode was also used to determine pH.

The Visual MINTEQ software version 3.1 was chosen as a freeware chemical equilibrium model for the calculation of metal concentration and activities of speciation, percentage distribution among dissolved and adsorbent species, and saturation index for each compound in the leaching solution. Moreover, to investigate the electrochemical stability of different redox states of Cu, S, and Mo as a function of pH, the Eh–pH diagram was drawn by HSC Chemistry software version 6.0.

2.4 Cyclic Voltammetry Measurement

The electrochemical system (Fig. 2) consists of three electrodes: a platinum wire as a counter electrode, a commercial Ag/AgCl saturated by KCl as a reference electrode, and a platinum wire as a working electrode, respectively. After each run, the working electrode was polished to a mirror-like surface using Al_2O_3 powder at a particle size of 0.3 μm. The electrodes were rinsed with bidistilled water after polishing. A stream of Argon gas was purged into each solution for 5 min before each scan for deoxygenation. In this experiment, open circuit potential (OCP) was measured when no current was flowing and no external voltage was applied. The electrochemical experiments were maintained at the open circuit or a predetermined potential at equilibrium time (30 s) to continue with a negative/positive going potential sweep from OCP in the direction of the expected half-reactions. To investigate the impact of the scanning rate, the sweep rates of 0.01, 0.05, and 0.1 V/s were carried out in the presence of 0.1 M KCl. In this research, the electrochemical behavior of leaching agents such as $CaCl_2$, $CuCl_2$, and $FeCl_3$ was analyzed individually and collectively in the acidic aqueous solution. Cyclic voltammetry measurement was performed using a potentiostat/galvanostat (Behpajooh, Iran).

2.5 Kinetic Study

In this research, for a better understanding of the leaching mechanism, a kinetic study was carried out in conducting with the experimental data. In this area, the shrinking core

Fig. 2 Electrochemical setup for analysis of leaching solution
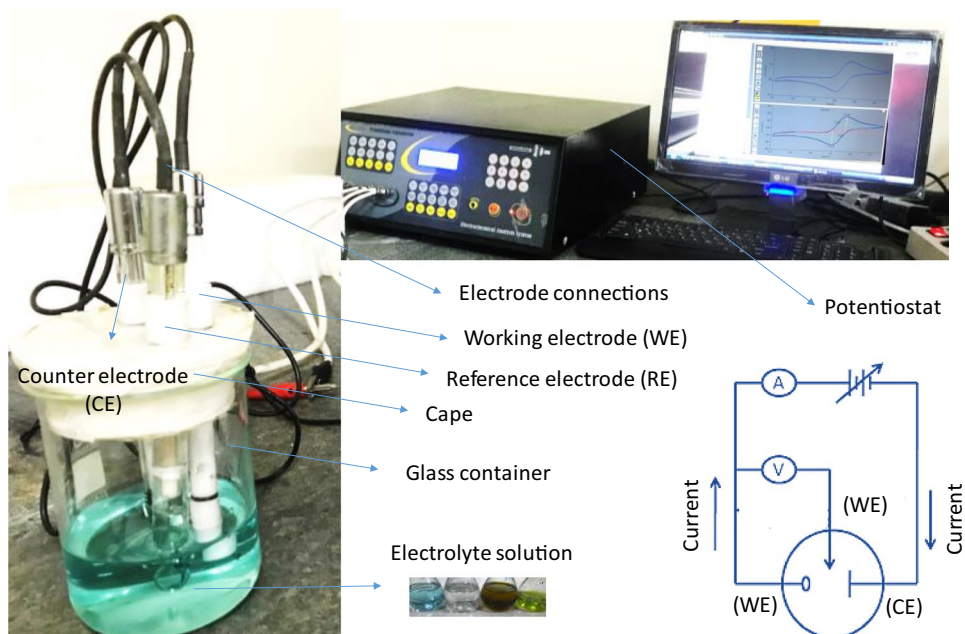
model was found to be the most important kinetic model for describing the leaching kinetics of metal ions [32].

The shrinking core model describes how the leaching process can be controlled by the following: I. the external diffusion of the leaching agent to the solution boundary layer; II. internal diffusion from the solution to the core surface (i.e., controlled through a solid product layer), or by performing a leaching reaction on the core surface [7].

Equations (1) and (2) can calculate the diffusion and chemical reaction control in the shrinking core model, respectively [8].

$$1 - \left(\frac{2}{3}\right) X - (1 - X)^{\frac{2}{3}} = k_d t \tag{1}$$

$$1 - (1 - X)^{\frac{1}{3}} = k_c t \tag{2}$$

where X is the reaction fraction after reactant at a given time (t), k_d and k_c are the reaction rate coefficients for diffusion and chemical reaction control, respectively. In order to diffusion control from reaction product layers, the reaction can be controlled by the unreacted core and the reaction product layer as shown in Eq. (3) [20].

$$\frac{1}{3}\ln(1 - X) - 1 + (1 - X)^{-\frac{1}{3}} = k_d \tag{3}$$

To determine the effect of temperature changes on the rate constant, Arrhenius equation can be used (Eq. (4)) [42]:

$$k = A \, \exp\left(-\frac{E_a}{RT}\right) \tag{4}$$

where A is the pre-exponential factor, E_a denotes the activation energy of the chemical reaction, R is the universal gas constant equal to 8.31 J/Kmol, and T is the absolute temperature associated with the reaction [6].

The value of activation energy can be helpful in determining the controlling mechanism. If the activation energy is lower than 20 kJ/mol, the reaction is controlled by the diffusion mechanism. However, values higher than 40 kJ/mol imply a chemically controlled reaction. The activation energy of between 20 and 40 kJ/mol indicates that the controlling mechanism is both chemical and diffusion reactions [17].

3 Results and Discussion

3.1 Physicochemical Characterizations of Molybdenum Concentrate Before Copper Dissolution

The results of the LPSA analysis for molybdenum concentrate are shown in Fig. 3. The particle size distribution
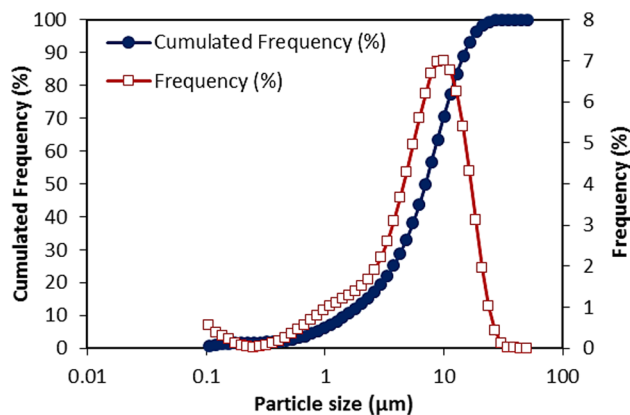

Fig. 3 Particle size distribution of molybdenum concentrate

Table 2 Peroxide fusion data of molybdenum concentrate compositions

Composition	wt.%	Composition	wt.%
Mo	46.38	SiO_2	0.98
S	40.28	Pb	<0.05
Fe_2O_3	5.18	P	<0.05
Cu	0.81	Zn	<0.05
CaO	0.32	Sr	<0.05
K_2O	0.18	Cr_2O_3	<0.05
MgO	0.13	TiO_2	<0.05
MnO	<0.05	BaO	<0.05
L.O.I	23.65		

of molybdenite was reported in terms of $d_{10} = 1.60$ µm, $d_{50} = 6.99$ µm, $d_{70} = 10.10$ µm, and $d_{90} = 16.53$ µm. The molybdenite particle size fraction represented the range of 0.09 to 53.20 µm.

In Table 2, the chemical compositions of molybdenum concentrate are shown. Based on the peroxide fusion result, the main chemical components belonged to Mo and S. However, the other impurities, including Fe_2O_3, Cu, CaO, K_2O, MgO, MnO, and SiO_2, were detected in molybdenite. The amounts of the other elements can be negligible. In this way, about 1 wt.% of molybdenite contains copper elements that need to be separated.

As shown in Fig. 4, the XRD pattern of molybdenum concentrate revealed the mineralogical composition and phases. The obtained results indicate that the molybdenum concentrate mainly contains molybdenite (MoS_2) with the diffraction at $2\theta = 14.5°$. In molybdenum concentrate, copper sulfide is mainly present in the forms of chalcopyrite ($CuFeS_2$) at $2\theta = 29.2°$, chalcocite (Cu_2S) at $2\theta = 37.2°$,

and covellite (CuS) at $2\theta = 32.7°$. Iron in this concentrate is present as pyrite (FeS_2) at $2\theta = 33.2°$, $37.1°$, and $56.2°$, and iron oxide (Fe_2O_3) at $2\theta = 32.9°$ and $62.9°$. In addition, quartz (SiO_2) is the other impure phase in the molybdenum concentrate at $39.6°$. Based on XRD and ICP-OES data, more than 90%wt. of molybdenum concentrate belonged to molybdenite and less than 5 wt.%. of this concentrate was composed of sulfide phases where chalcopyrite was the main impurity.

To clarify the composition of the copper minerals presented in the molybdenum concentrate, the microscopic study was carried out and shown in Fig. 5. The results showed that most minerals are liberated without any interlocking. However, in some cases, there is a slight interlocking between molybdenite and chalcopyrite.

The morphological and semi-qualitative analyses of the molybdenite sample were given by FESEM-EDS. Fig. 6a illustrates the small and thin layers of molybdenum

with a blade-shaped particle. Based on the percentages of O, Si, S, Cl, Ca, Fe, Cu, and Mo elements (Fig. 6b) and the EDS-mapping distribution of these elements (Fig. 6c), molybdenum concentrate is primarily composed of molybdenum, iron, and copper related to molybdenite, pyrite, and copper sulfide minerals (such as chalcopyrite, chalcocite, and covellite).

3.2 Effect of Different Leaching Conditions in Lab-Scale

The effect of various concentrations of $CaCl_2$ (0–3 M) on the copper sulfide compounds (especially chalcopyrite) dissolution was investigated. The experiment was carried out in the solution of 1 M HCl, at the temperature of 75 °C, 500 rpm, 0.5 M $FeCl_3$ concentration, an initial $CuCl_2$ concentration of 0.05 M, and S:L ratio of 1:10. As shown in Fig. 7a, increasing the $CaCl_2$ concentration had

Fig. 4 XRD pattern of the molybdenum concentrate
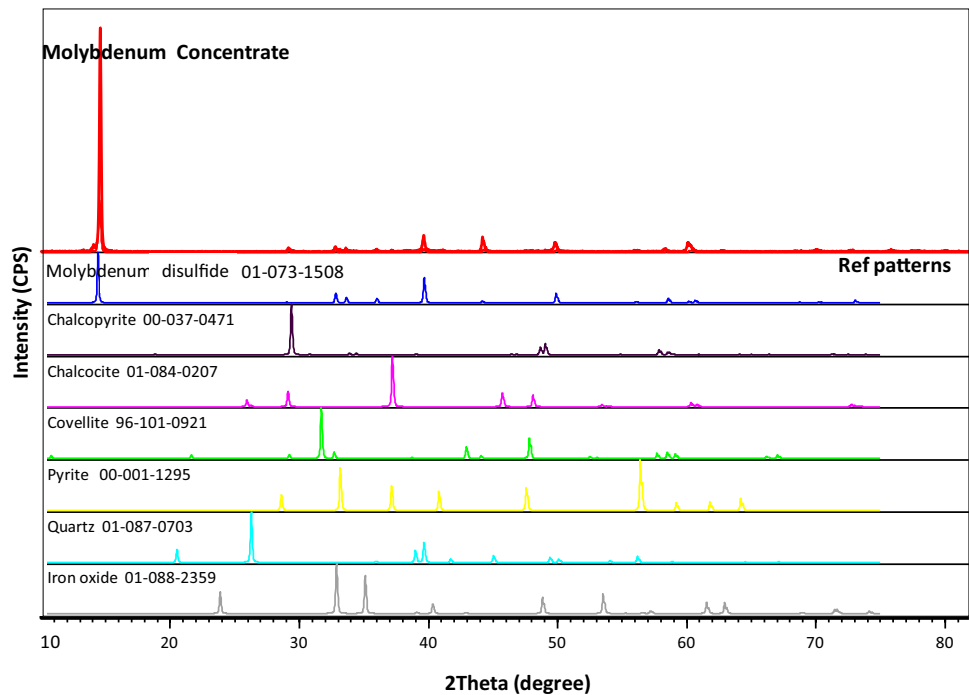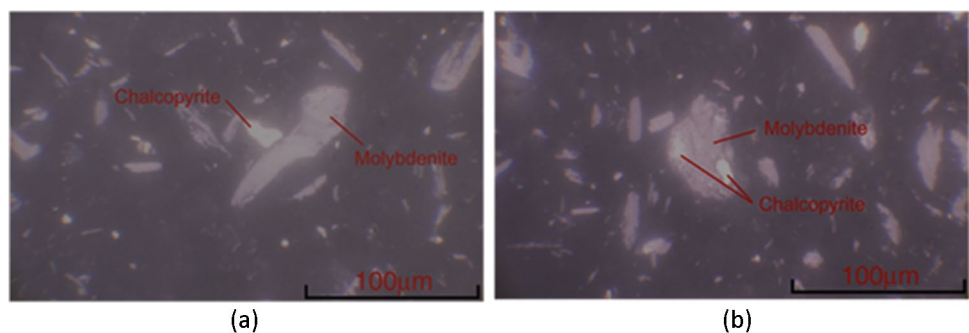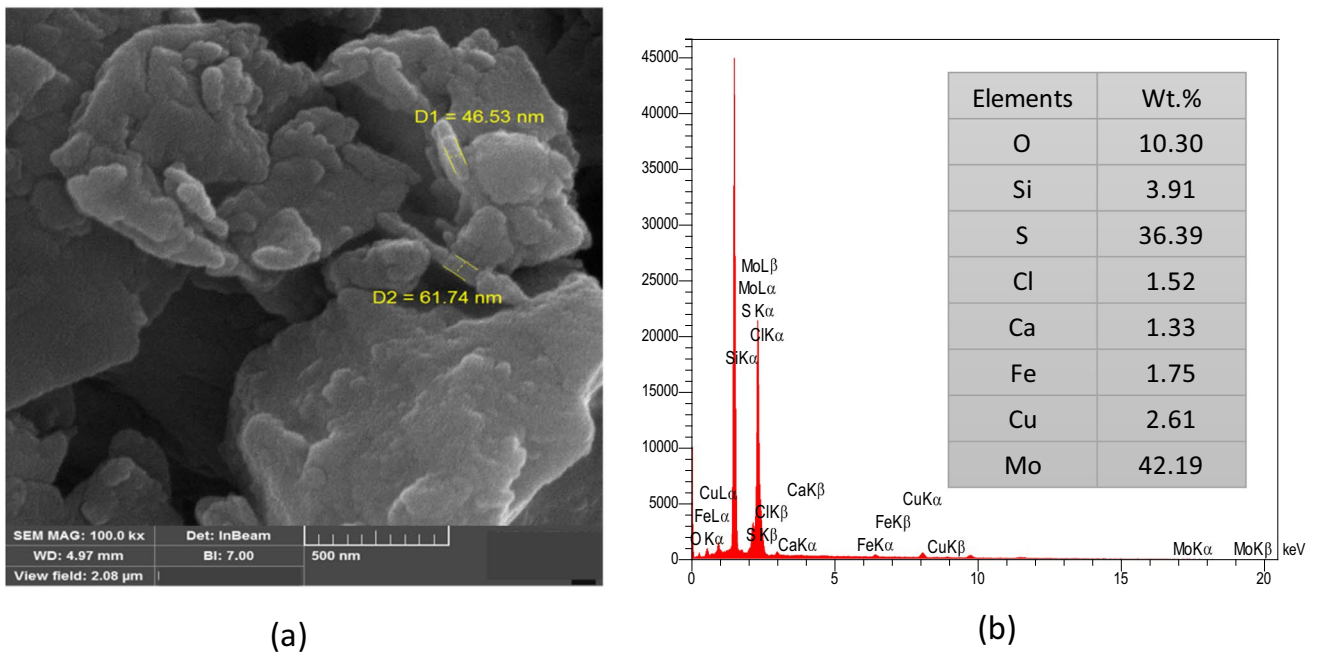

Fig. 5 Presence of copper sulfide in molybdenum concentrate **a** without interlocking and **b** possible interlocking of chalcopyrite with molybdenite using reflected light-parallel polarization

(a)

(b)

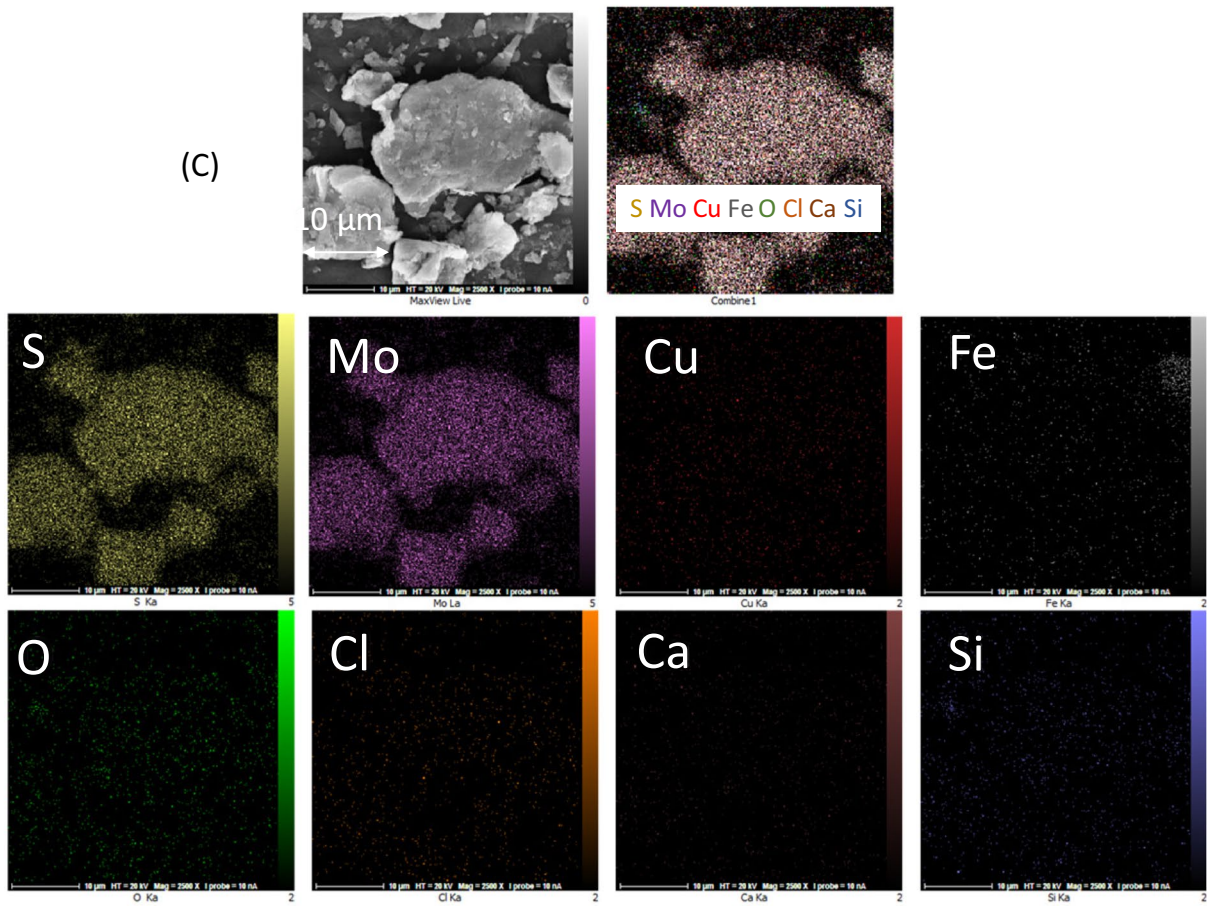| Elements	Wt.%
O	10.30
Si	3.91
S	36.39
Cl	1.52
Ca	1.33
Fe	1.75
Cu	2.61
Mo	42.19

(C)

Fig. 6 **a** FESEM image; **b** elemental analysis and **c** EDS mapping of molybdenum concentrate
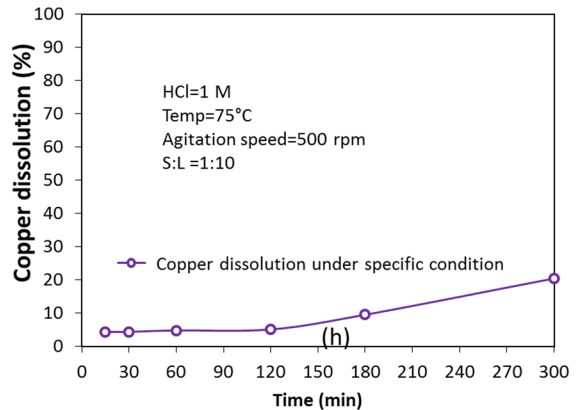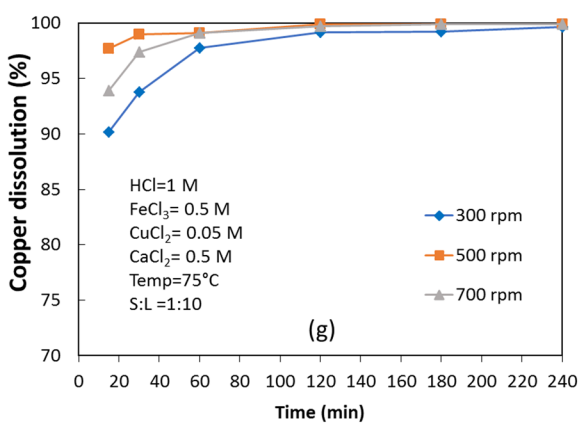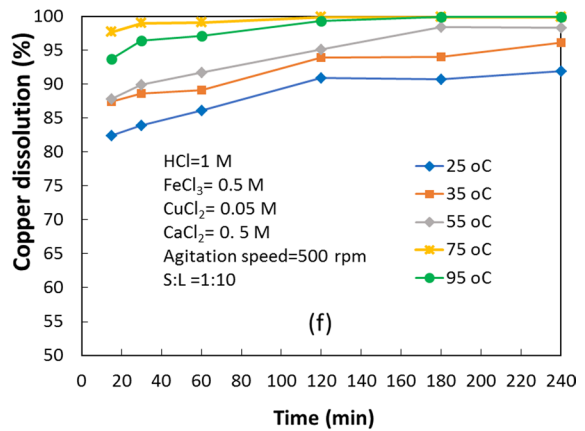
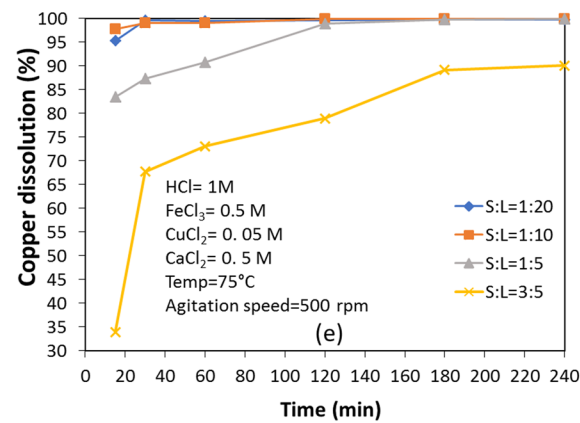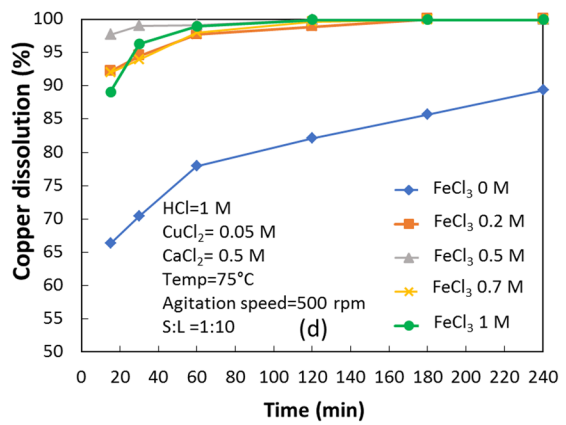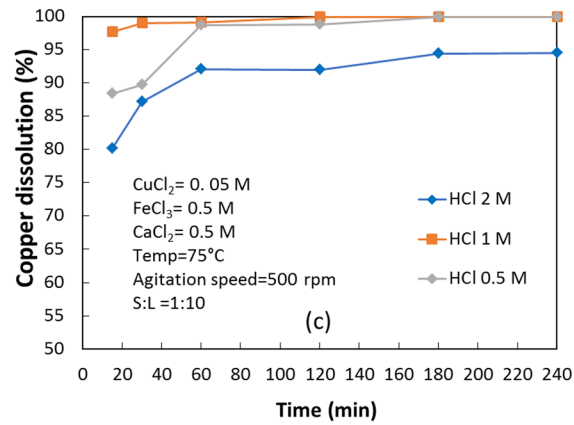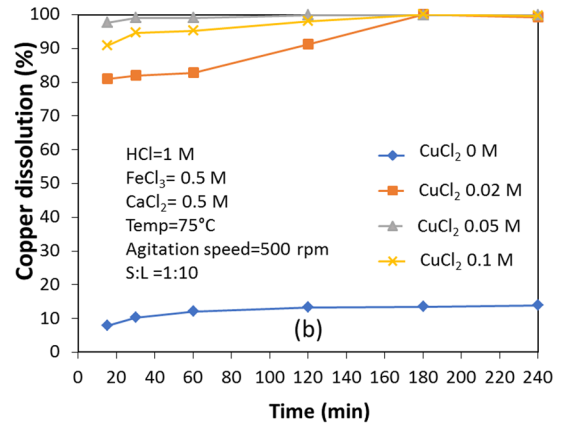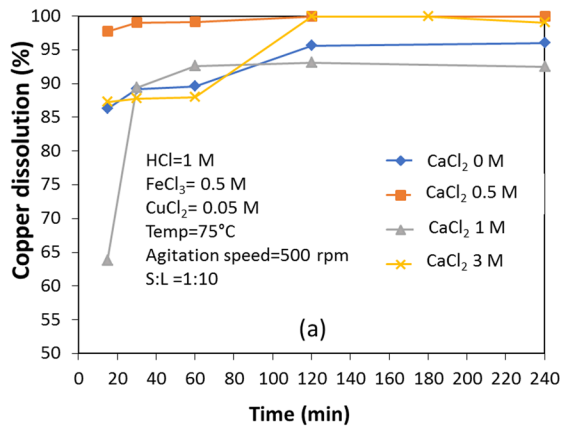◀**Fig. 7** Effect of **a** CaCl$_2$ concentration, **b** CuCl$_2$ concentration, **c** HCl concentration, **d** FeCl$_3$ concentration, **e** S:L ratio, **f** temperature, **g** agitation speed, and **h** copper dissolution under specific condition

a positive effect on copper dissolution only up to 0.5 M. After that, a significant effect on copper dissolution was not observed. During 60-min leaching, maximum copper recovery was obtained up to 99% and the copper dissolution was slightly changed after 60 min. The presence of CaCl$_2$ could be helpful for copper dissolution by increasing the chlorination degree and ionic strength of the solution and influencing the refractory copper sulfide (chalcopyrite) dissolution.

The effect of initial CuCl$_2$ concentration (0–0.1 M) on the leaching of copper sulfides was studied in solutions containing 1 M HCl, 0.5 M FeCl$_3$, 0.5 M CaCl$_2$, at 75 °C, 500 rpm and S:L ratio of 1:10. Based on the results depicted in Fig. 7b, the CuCl$_2$ concentration of 0.05 M was selected as the optimum value at 60 min. As shown in Fig. 7b, the absence of CuCl$_2$ indicated a significant reduction in copper dissolution to 13%. Oxidizing effect of CuCl$_2$ besides its catalytic role in the dissolution of copper was significant.

Copper leaching behavior was studied by varying HCl concentrations (0.5–2 M). Fig. 7c depicted the copper recovery under FeCl$_3$ concentration of 0.5 M, 0.5 M CaCl$_2$, 0.05 M CuCl$_2$ at 75 °C, 500 rpm and S:L ratio of 1:10. 1 M HCl represented the optimum amount for maximum copper dissolution at 60-min leaching time.

The experiments on the effect of the FeCl$_3$ concentration (0 − 1 M) on copper dissolution were carried out using 1 M HCl, at 75 °C, 0.5 M CaCl$_2$ concentration, CuCl$_2$ concentration of 0.05 M, at 500 rpm and S:L ratio of 1:10. As shown in Fig. 7d, the increase in FeCl$_3$ concentration improved copper dissolution. However, the FeCl$_3$ concentration of 0.5 M showed a desirable amount to reach maximum yield. Based on the mineralogical results, the high values of copper sulfide minerals belonged to chalcopyrite; therefore, the presence of FeCl$_3$ oxidative agent could be effective to obtain maximum copper dissolution. In the other study reported by Lessard and Shekhter [25], the thermodynamic modeling of chalcopyrite dissolution indicated that for complete copper leaching with minimum molybdenite leaching, 0.5 M FeCl$_3$ concentration was sufficient.

The solid/liquid ratio effect was studied in the solution of 0.5 M HCl 0.5 M FeCl$_3$, 0.5 M CaCl$_2$, and 0.05 M CuCl$_2$ at 75 °C and in various ratios (1:20, 1:10, 1:5, and 3:5). As shown in Fig. 7e, the solid/liquid ratio affected the copper extraction significantly. The dissolution curves showed that the maximum copper recovery was obtained in dilute suspension and the ratio of 1:10 was chosen as an optimum amount.

As shown in Fig. 7f, the copper recovery was investigated at different temperatures (25–95 °C) under 1 M HCl, 0.5 M FeCl$_3$, 0.5 M CaCl$_2$, 0.05 M CuCl$_2$ concentration, at 500 rpm and S:L ratio of 1:10. During 60-min leaching, the temperature represented a considerable effect on the leaching rate by increasing the temperature from 25 to 75 °C to achieve more than 99% copper recovery.

The effect of the agitation speed (300, 500, and 700 rpm) on molybdenum concentrate leaching was studied under HCl concentration of 1 M, FeCl$_3$ concentration of 0.5 M, 0.5 M CaCl$_2$, 0.05 M CuCl$_2$ at 75 °C and S:L ratio of 1:10. Generally, the copper recovery was slightly increased with increasing agitation speed during 60 min (Fig. 7g). This result represented that mass transfer may not play an important role in the leaching process at higher agitation speeds. Accordingly, an agitation speed of 500 rpm was selected as an optimum value for maximum copper leaching.

In this study, the effect of each leaching agent on copper dissolution, in the absence of copper, calcium, and iron chloride for copper dissolution, was also evaluated. The results are given in Fig. 7h and revealed that the copper recovery was located at the lowest level when the CuCl$_2$, FeCl$_3$, and CaCl$_2$ were absent.

3.3 Chemical Equilibrium Modeling of Copper Leaching Process

Visual MINTEQ is a chemical equilibrium free software that can be used to calculate metal speciation, solubility, solid equilibrium, and the mineral dissolved phases in aqueous systems [3]. Therefore, in this study, Visual MINTEQ version. 3.1 was used to simulate the concentrations of aqueous inorganic species, the saturation indexes (SI: the logarithmic ratio of ion activity product to solubility coefficient for each compound), and the percentage distribution of dissolved species in the leaching solution. The chemical equilibrium modeling results provide a theoretical basis for a better understanding of leaching reagent behavior and aqueous reactions for copper dissolution in the laboratory.

The simulation was performed at 75° for 50 g of molybdenum concentrate in 0.5 L of solution with HCl = 1 M, FeCl$_3$ = 0.5 M, CuCl$_2$ = 0.05 M, and CaCl$_2$ = 0.5 M. The results of the simulation data are given in Table 3. The obtained results represented the probable molybdenite dissolution and the formation of various types of copper sulfide, iron chloride, and copper chloride complexes in the leaching solution that can cover the surface of copper sulfide minerals in molybdenum concentrate.

According to the results of the saturation index in Table 4, the precipitation in the leaching solution has theoretically happened. A negative value of the saturation index suggests that compounds are under saturation and a positive value of the saturation index shows the formation of precipitation. Therefore, it is theoretically possible to form a precipitated layer on the surface of copper sulfide minerals during the leaching process (i.e., as a passive layer).

Table 3 Percentage distribution among dissolved species

Component	% of total concentration	Species name
MoO_4^{2-}	0.03	$H_2Mo_6O_{21}^{4-}$
	0.01	$HMoO_4^-$
	3.50	$MoO_3(H_2O)_3(aq)$
	0.06	$HMo_7O_{24}^{5-}$
	0.85	$H_3Mo_8O_{28}^{5-}$
	95.55	$Mo_8O_{26}^{4-}$
HS^-	100.00	H_2S (aq)
Cl^-	85.69	Cl^-
	0.08	$CuCl^+$
	2.40	$CuCl_2$ (aq)
	0.30	$CuCl_3^-$
	0.01	$CuCl_4^{2-}$
	11.52	$FeCl^{2+}$
Fe^{3+}	0.27	Fe^{3+}
	99.73	$FeCl^{2+}$
Cu^{2+}	4.73	Cu^{2+}
	5.39	$CuCl^+$
	82.88	$CuCl_2$ (aq)
	6.81	$CuCl_3^-$
	0.19	$CuCl_4^{2-}$
Ca^{2+}	100.00	Ca^{2+}

Table 4 Saturation index data for leaching solution

Mineral	Saturation index
Atacamite	-10.45
$CaMoO_4(s)$	-2.604
$CaS(s)$	-18.935
Covellite	10.576
$Cu(OH)_2(s)$	-10.848
$CuMoO_4(s)$	0.717
Cupric Ferrite	-9.954
$Fe(OH)_{2.7}Cl_{.3}(s)$	-0.251
Ferrihydrite	-4.079
Ferrihydrite (aged)	-3.569
Goethite	-2.259
$H_2MoO_4(s)$	2.261
Hematite	-1.809
Lepidocrocite	-4.664
Lime	-29.154
Maghemite	-12.859
Melanothallite	-6.797
$MoO_3(s)$	-1.27
Portlandite	-20.914
Powellite	-1.929
Tenorite(am)	-9.64
Tenorite(c)	-8.79

To further investigate the copper dissolution beside the possibility of molybdenum dissolution in the leaching process, the values of redox potential and pH of the solution in optimum conditions are measured and listed in Table 5.

As shown in Table 5, the main mechanism for chalcopyrite as a main copper sulfide mineral in molybdenum concentrate in acidic solution with the presence of $CuCl_2$, and $CaCl_2$ (as a just spectator) could be followed by Eq. (5) or Eqs. (6) and (7). Equation (5) is reported to represent the chalcopyrite dissolution in $FeCl_3$. This system is faster and more aggressive than the other ferric salts [27].

$$CuFeS_2 + 4Fe^{3+} \rightarrow Cu^{2+} + 5Fe^{2+} + 2S^o \qquad (5)$$

Equation (5) can also be represented by the following half-cell reaction pair (Eqs. (6) and (7)):

$$CuFeS_2 \rightarrow Cu^{2+} + Fe^{2+} + 2S^o + 4e^- \qquad (6)$$

$$4Fe^{3+} + 4e^- \rightarrow 4Fe^{2+} \qquad (7)$$
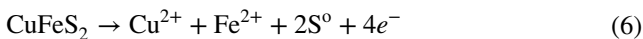
Equation (8) is shown the use of $CuCl_2$ as an oxidant where chalcopyrite is reported to dissolve [34].

$$CuFeS_2 + 3Cu^{2+} \rightarrow 4Cu^+ + Fe^{2+} + 2S^o \qquad (8)$$
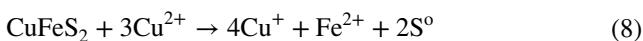
As shown in Eqs. (9) and (10), half-cell reactions for chalcopyrite dissolution are followed as:

$$CuFeS_2 \rightarrow Cu^+ + Fe^{2+} + 2S^o + 4e^- \qquad (9)$$

$$3Cu^{2+} + 3e^- \rightarrow 3Cu^+ \qquad (10)$$
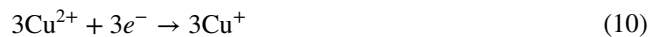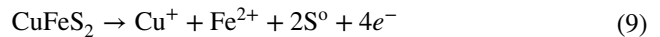
The low pH value obtained from the experiment proved the consumption of elemental sulfur (i.e., formed from copper sulfide leaching), at higher temperatures (about 70–80 °C). Equation (11) showed the reason for extensive acidic media during leaching solution [25]:

$$S^o + 4H_2O + 6FeCl_3 \rightarrow H_2SO_4 + 6FeCl_2 + 6HCl \qquad (11)$$

In this study, for a better understanding of the probable dissolution of Mo in leaching solution, the Eh–pH diagram of the Mo-S-H$_2$O system was obtained at 25 and 75 °C according to the concentrations of Mo and S in molybdenum ore by the HSC

Table 5 Solution potential and pH of leaching solution at optimum condition

| Leaching time (min)	Redox potential (V, SHE)	pH
15	0.659	0.07
30	0.624	0.07
60	0.617	0.06
120	0.607	0.06
240	0.608	0.01

**Fig. 8** Eh–pH diagram for Mo-S-H$_2$O system at 25 and 70 °C
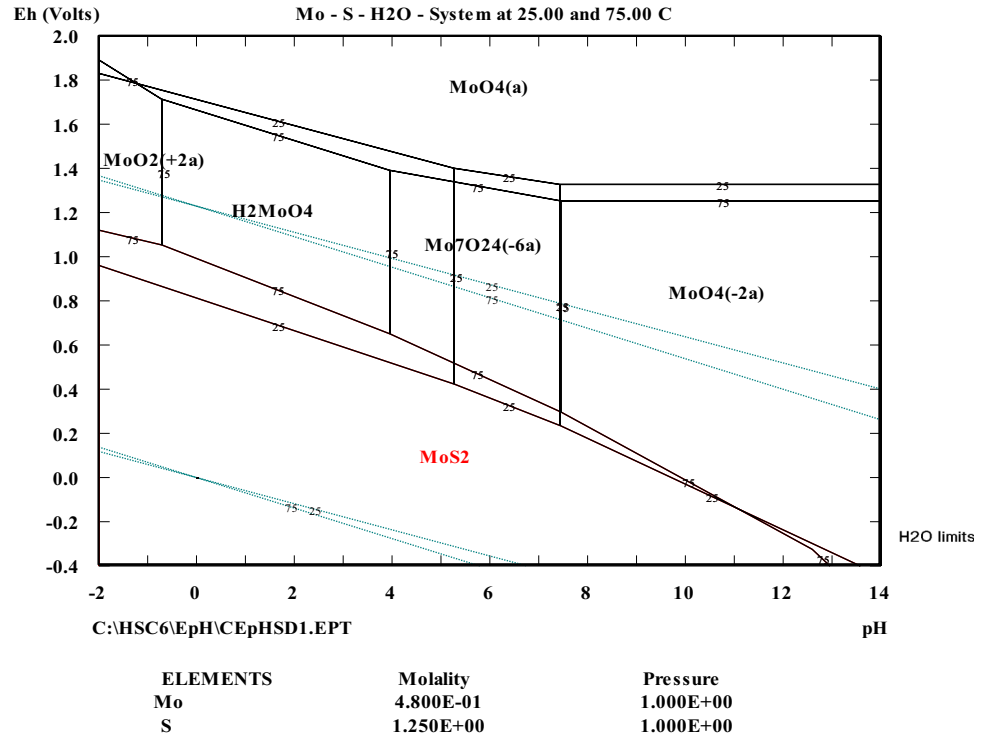
Chemistry database. As shown in Fig. 8, at 75 °C and a redox potential of less than 900 mV (SHE) and pH less than 1, the molybdate species were located in a stable form (MoS$_2$). Therefore, the dissolution of Mo in the optimum leaching conditions in this study (i.e., Eh$\approx$600 mV (SHE), 0.01 < pH < 0.07, and 75 °C) is impossible. Therefore, the formation of H$_2$Mo$_6$O$_{21}$$^{4-}$, HMoO$_4$$^-$, MoO$_3$(H$_2$O)$_3$(aq), HMo$_7O_{24}$$^{5-}$, H$_3Mo_8O_{28}$$^{5-}$, and Mo$_8O_{26}$$^{4-}$, based on Visual MINTEQ modeling, has not happened in the leaching solution. Moreover, the presence of CuCl$_2$, CuCl$_3$$^-$, and CuCl$_4$$^{2-}$ plays an important role in the dissolution

rates of copper. As reported by Yoo et al. [52], the distribution of copper ions with increasing chloride concentration plays an important role in chalcopyrite dissolution. In this research, the role of CaCl$_2$ and CuCl$_2$ beside FeCl$_3$ and acidic medium caused the increase in the chloride concentration, so cuprous ion species such as CuCl, CuCl$_2$$^-$, CuCl$_3$$^{2-}$, and CuCl$_3$$^{2-}$ are formed as chlorocuprate(I) ions, and the standard potential between cupric and cuprous species also increases. In addition, chalcopyrite is leached faster when increasing the Cu^{2+}/Cu$^+$ ratio as the solution becomes more concentrated in Cl$^-$ ions. Therefore,
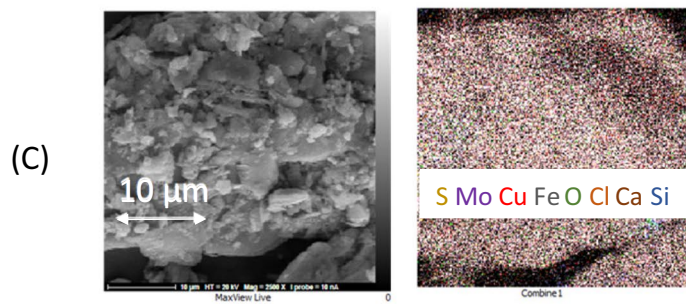
Fig. 9 3D XRD patterns of molybdenum concentrate before and after leaching
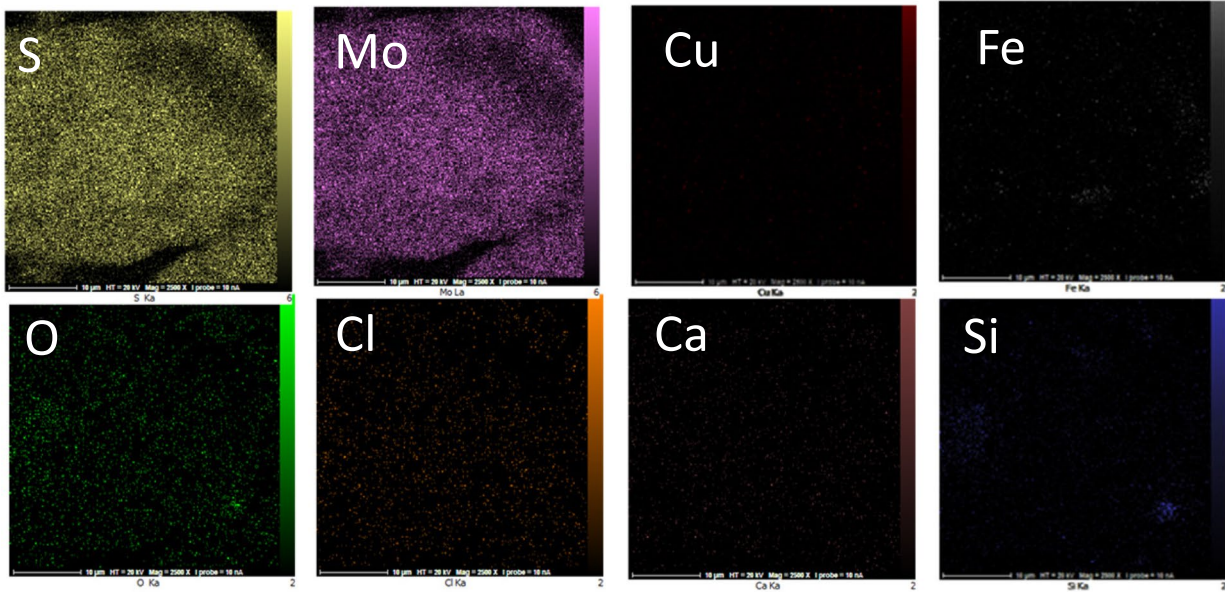
(a)

Elements	Wt.%
O	10.18
Si	3.09
S	34.49
Cl	1.47
Ca	0.95
Fe	1.46
Cu	0.38
Mo	47.98
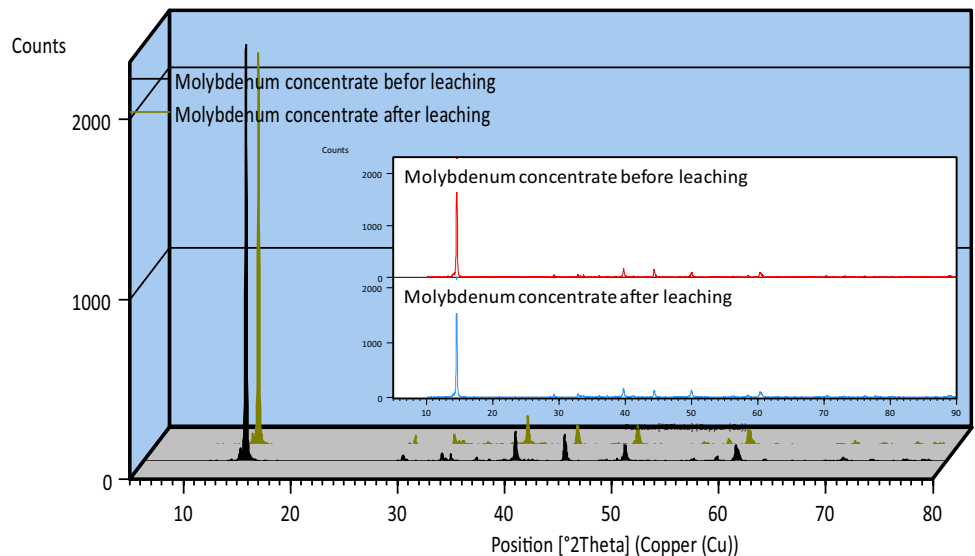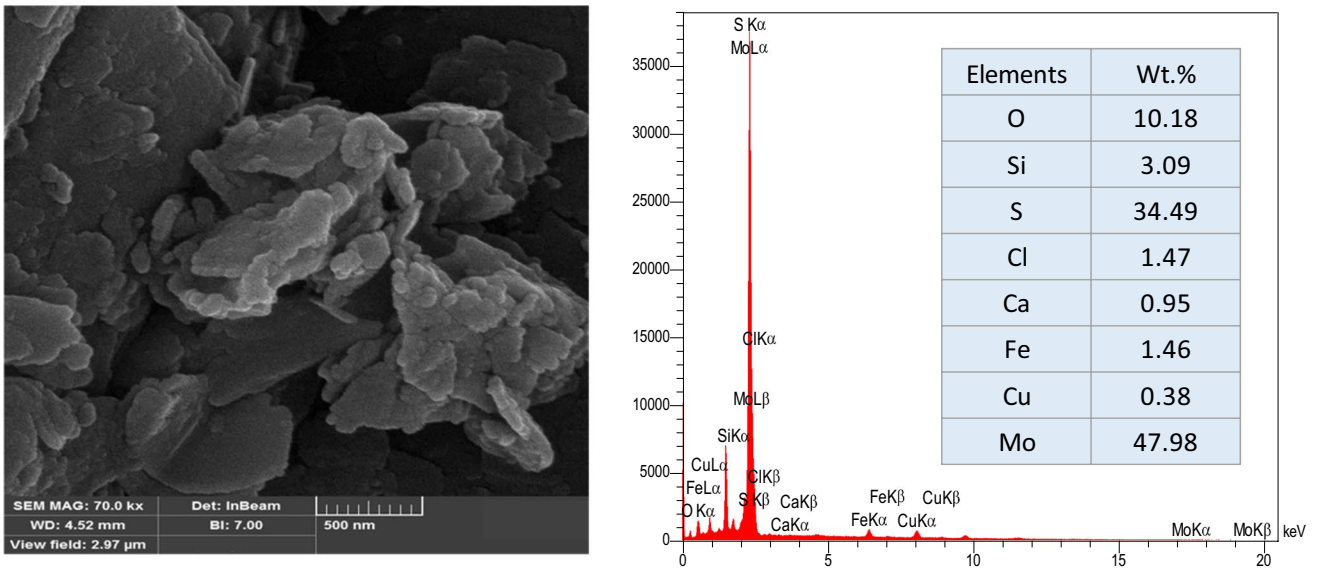
(b)

(C)

Fig. 10 **a** FESEM image; **b** elemental analysis, and **c** EDS mapping of molybdenite after copper dissolution

as reported in Eq. (10), the high Cu^{2+}/Cu^+ ratio increases the dissolution of chalcopyrite in Eq. (9) [4].

3.4 Physicochemical Characterizations of Molybdenum Concentrate After Copper Dissolution

In this research, to investigate the molybdenum dissolution, further study was also performed on the leaching residue. The results of ICP-OES data for residue under optimum conditions showed only 0.03 wt.% dissolution of Mo. The XRD results of the leaching residue confirmed the ICP-OES analysis data. Accordingly, the molybdenum was not dissolved during the leaching process. The preservation of the main peaks of molybdenum at $2\theta = 14.5°$ was illustrated in Fig. 9.

Moreover, to study the reduction of the copper amount in the leaching residue, the FESEM-EDS analysis was used. As

shown in Fig. 10a–c, the dissolution of copper sulfide minerals such as chalcopyrite, chalcocite, and covellite resulted in a significant decrease in Cu values and their distributions in EDS mapping.

3.5 Electrochemical Behavior of Leaching Agents

In this study, CV is a powerful electrochemical technique employed to investigate the reduction and oxidation processes of molecular species in leaching solution influenced on the leaching process. The CV scans of the leaching solution containing 0.05 M $CuCl_2$, 1 M HCl, and 0.1 M KCl as supporting electrolytes at 25 °C are shown in Fig. 11a. In the catholic peaks, the peaks started from the onset potential of $-0.22, -0.29$, and -0.32 V (Ag/AgCl) at different scan rates of 0.01, 0.05, and 0.1 V/s are related to the formation of the solid Cu on the working electrode surface (the reduction of Cu^+ to Cu) [21]. In the reverse
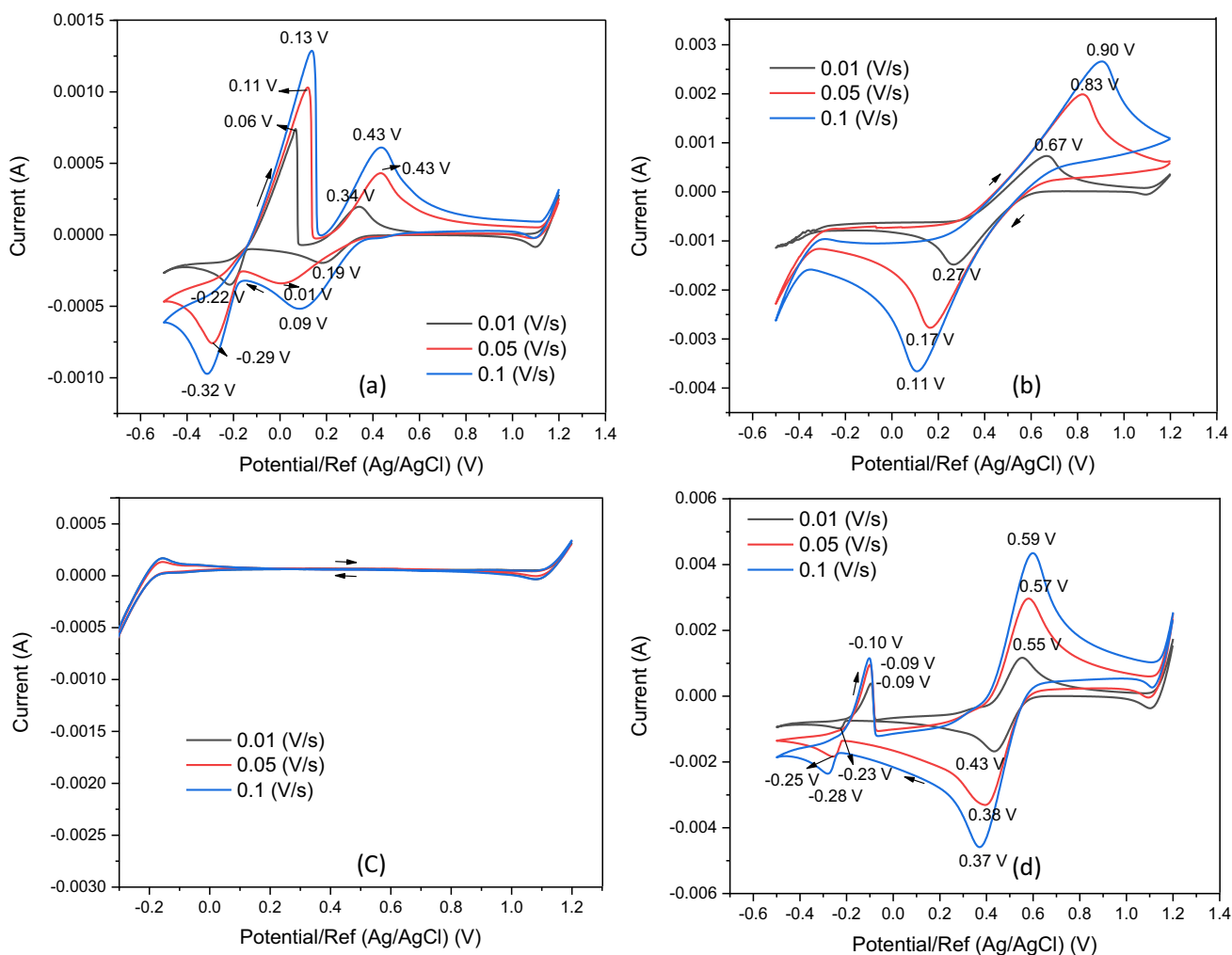

Fig. 11 Cyclic voltammograms of leaching solutions each containing **a** 0.05 M $CuCl_2$, **b** 0.5 M $FeCl_3$, **c** 0.5 M $CaCl_2$, and **d** 0.05 M $CuCl_2$, 0.5 M $FeCl_3$, 0.5 M $CaCl_2$ in 1 M HCl, 0.1 M KCl as supporting electrolyte at 25 °C

scan, anodic peaks started from the potential of 0.06, 0.11, and 0.13 V (Ag/AgCl) at different scan rates of 0.01, 0.05, and 0.1 V/s are related to the change of Cu to Cu^+ species, and the second peaks are located at 0.34, 0.43, and 0.43 V (i.e., at different scan rates of 0.01, 0.05, and 0.1 V/s) belong to the change of Cu^+ to Cu^{2+} species [18]. The peaks located at 0.19, 0.01 and 0.09 V (Ag/AgCl) (i.e., at different scan rates of 0.01, 0.05, and 0.1 V/s) in the cathodic scan belong to the reduction of Cu^{2+} to Cu^+ [33]. According to the electrochemical investigation, at leaching conditions of about 0.4 V (Ag/AgCl) and 1 M HClCl^- ions could react with copper ions to form complex anions such as $CuCl_3^-$ and $CuCl_4^{2-}$, which could affect the chalcopyrite leaching process [16].

The effect of the $FeCl_3$ agent was also investigated in a solution containing 0.5 M $FeCl_3$, 1 M HCl, 0.1 M KCl as a supporting electrolyte at 25 °C (Fig. 11b). Fe^{3+} ions are reduced to Fe^{2+} in cathodic reaction at potentials of 0.27,

0.17, and 0.11 V (Ag/AgCl) and scan rates of 0.01, 0.05, and 0.1 V/s. On the reverse scan, at potentials of 0.67, 0.83, and 0.90 V (Ag/AgCl), the oxidation of Fe^{2+} to Fe^{3+} is marked at different scan rates of 0.01, 0.05, and 0.1 V/s respectively [23].

As shown in Fig. 11c, the leaching solution containing 0.5 M $CaCl_2$, 1 M HCl, 0.1 M KCl as a supporting electrolyte at 25 °C shows no significant cathodic peaks. It means that $CaCl_2$ does not react with HCl and it is a water-soluble ionic salt. On the other hand, it means that the $CaCl_2$ is not an electroactive species in leaching solution and it affects the process through non-oxidative reactions or mass transfer.

Figure 11d exhibits the CV attained in a mixture of leaching agents (i.e., 1 M HCl, 0.5 M $FeCl_3$, 0.05 M $CuCl_2$, 0.5 M $CaCl_2$, 0.1 M KCl as a supporting electrolyte at 25 °C). The peaks related to cathodic reactions of Cu^+ to Cu are observed at $-0.23, -0.25, -0.28$ V (Ag/AgCl) and the reduction of Fe^{3+} to Fe^{2+} (i.e., which could be overlapped with the reduction of
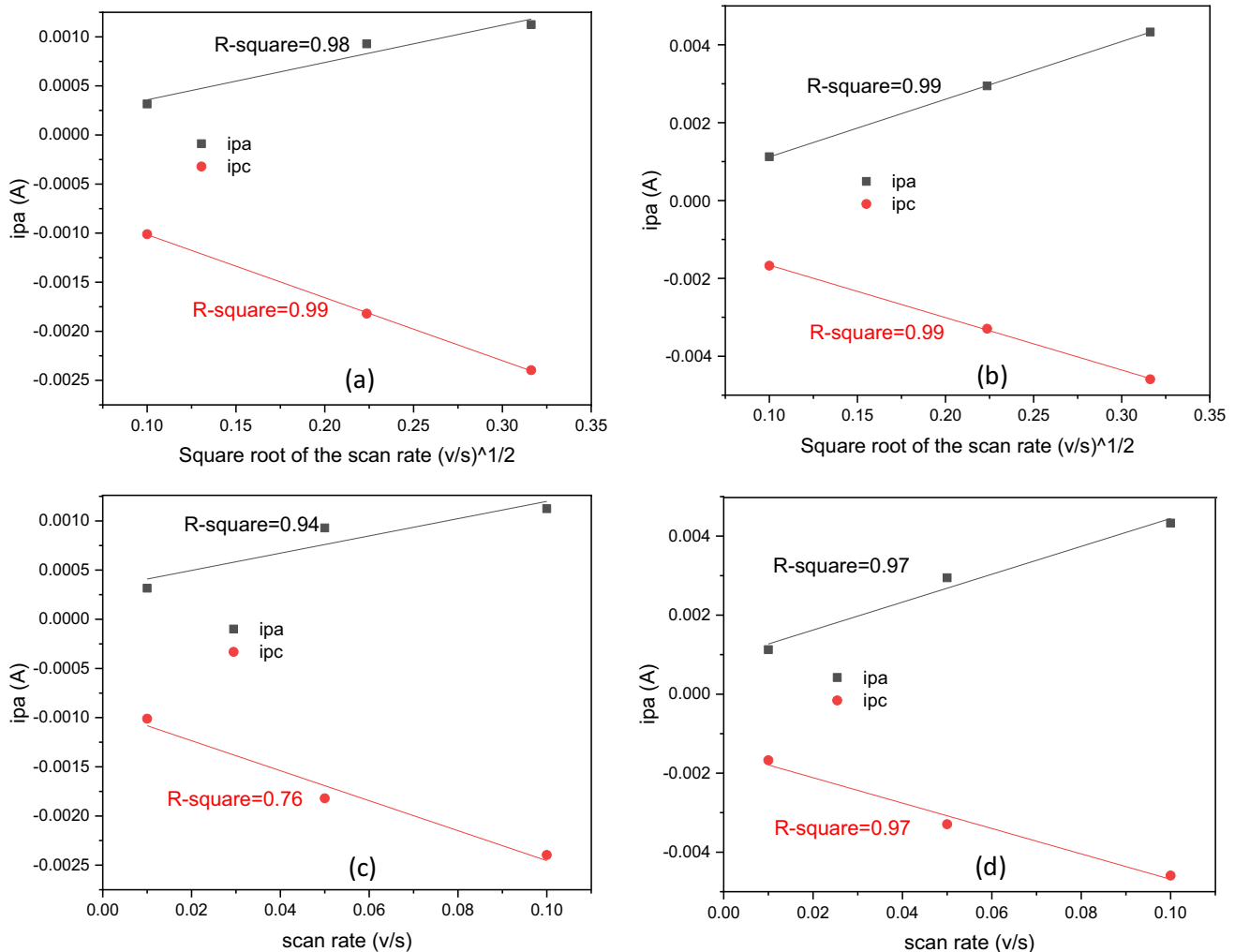

Fig. 12 The relation between peak current and **a** the square root of the scan rate for redox peaks of copper chloride, **b** the square root of the scan rate for redox peaks of ferric chloride, **c** the scan rate for redox peaks of copper chloride, and **d** the scan rate for redox peaks of ferric chloride

Table 6 The amount of lnkd at different temperatures

T (K)	1000/T	Kd	ln Kd
298	3.356	0.002	−6.215
308	3.247	0.003	−5.991
328	3.049	0.004	−5.521
348	2.874	0.019	−3.974
368	2.717	0.020	−3.922

Cu^{2+} to Cu^+) is also shown at 0.43, 0.38, and 0.37 V (Ag/AgCl) at different scan rates of 0.01, 0.05, and 0.1 V/s respectively. Moreover, on the reverse scan, at different scan rates of 0.01, 0.05, and 0.1 V/s, in these cyclic voltammograms, the peaks belong to the anodic reaction for changing of Cu to Cu^+ are detected at −0.09, −0.09, and −0.10 V (Ag/AgCl). The oxidation of Fe^{2+} to Fe^{3+} (i.e., which could be overlapped with the oxidation of Cu^+ to Cu^{2+}) is observed at 0.55, 0.57, and 0.59 V (Ag/AgCl) at 0.01, 0.05, and 0.1 V/s respectively. From another point of view, a higher $FeCl_3$ concentration in the sample containing $CuCl_2$ changes the locations of the peaks in comparison

with the individual solutions. In this area, as mentioned before, the formation of chlorocuprate(I) ions are probable to derive the leaching process.

The results of voltammetry studies also indicate that the solution potential oxidation of Cu^+ to Cu^{2+} is coupled to the higher formal potential of the Fe^{3+}/Fe^{2+} couple. The importance of such reaction can be understood considering the fact that despite Fe^{3+} is a thermodynamically stronger oxidant than Cu^{2+}, the rate of cathodic reduction of Cu^{2+} is probably greater than that of Fe^{3+} on the chalcopyrite surface [35]. Accordingly, the presence of Cu^{2+}/Cu^+ redox couple, which is only stable at the high concentration of chloride, can significantly affect the kinetic of chalcopyrite oxidation. These assumptions were evaluated through the leaching experiments in the following part.

The CV analysis could determine the diffusion-controlled and the surface-controlled redox reactions. The scan rate of the experiment controls the rate of the applied potential for scanning. When it is fast, a decrease in the size of the diffusion layer has been carried out and the higher currents
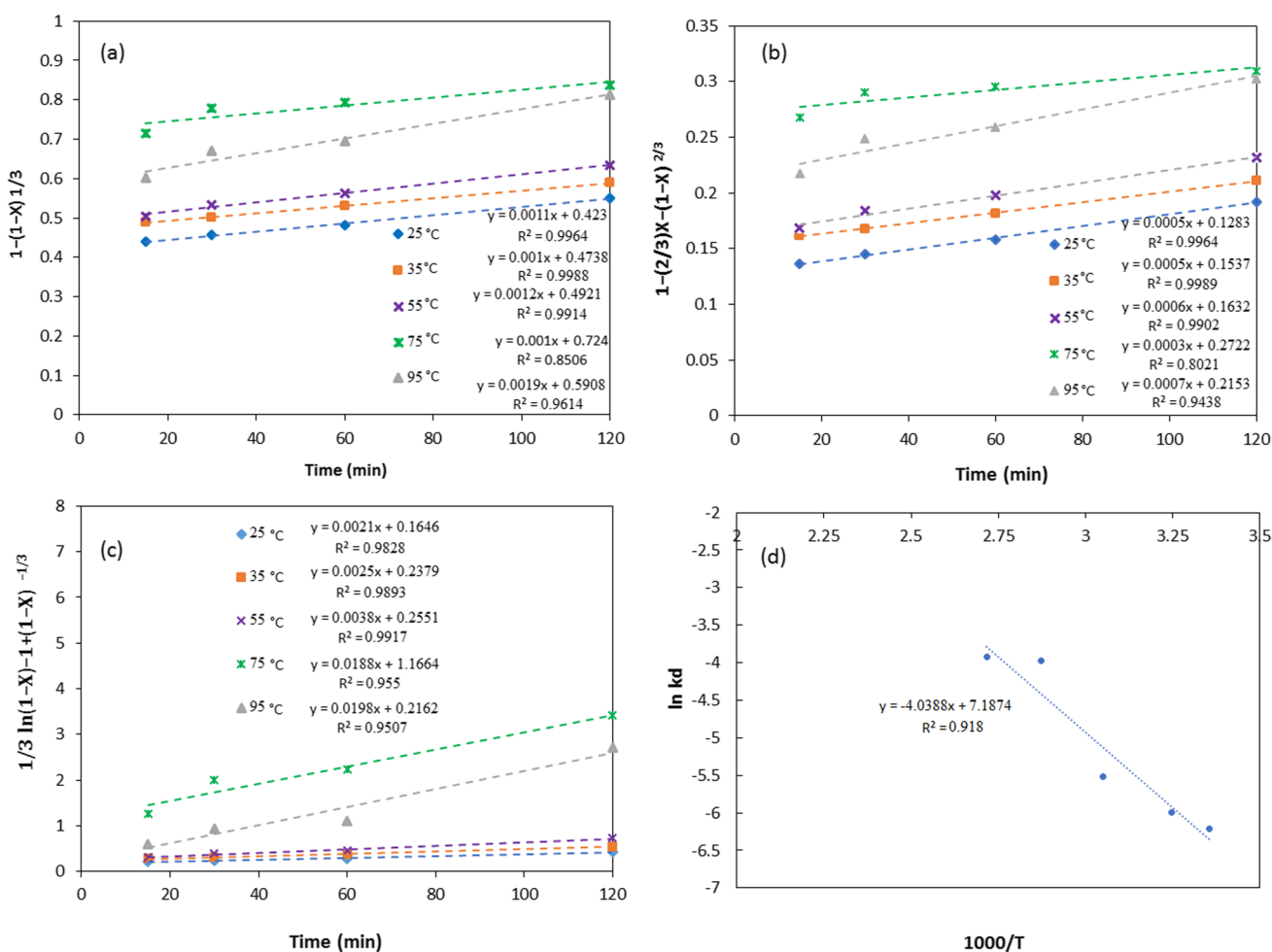

Fig. 13 Kinetic plots of copper dissolution based on **a** surface chemical reaction, **b** diffusion the product layer, **c** diffusion control from reaction product layers, and **d** Arrhenius plot
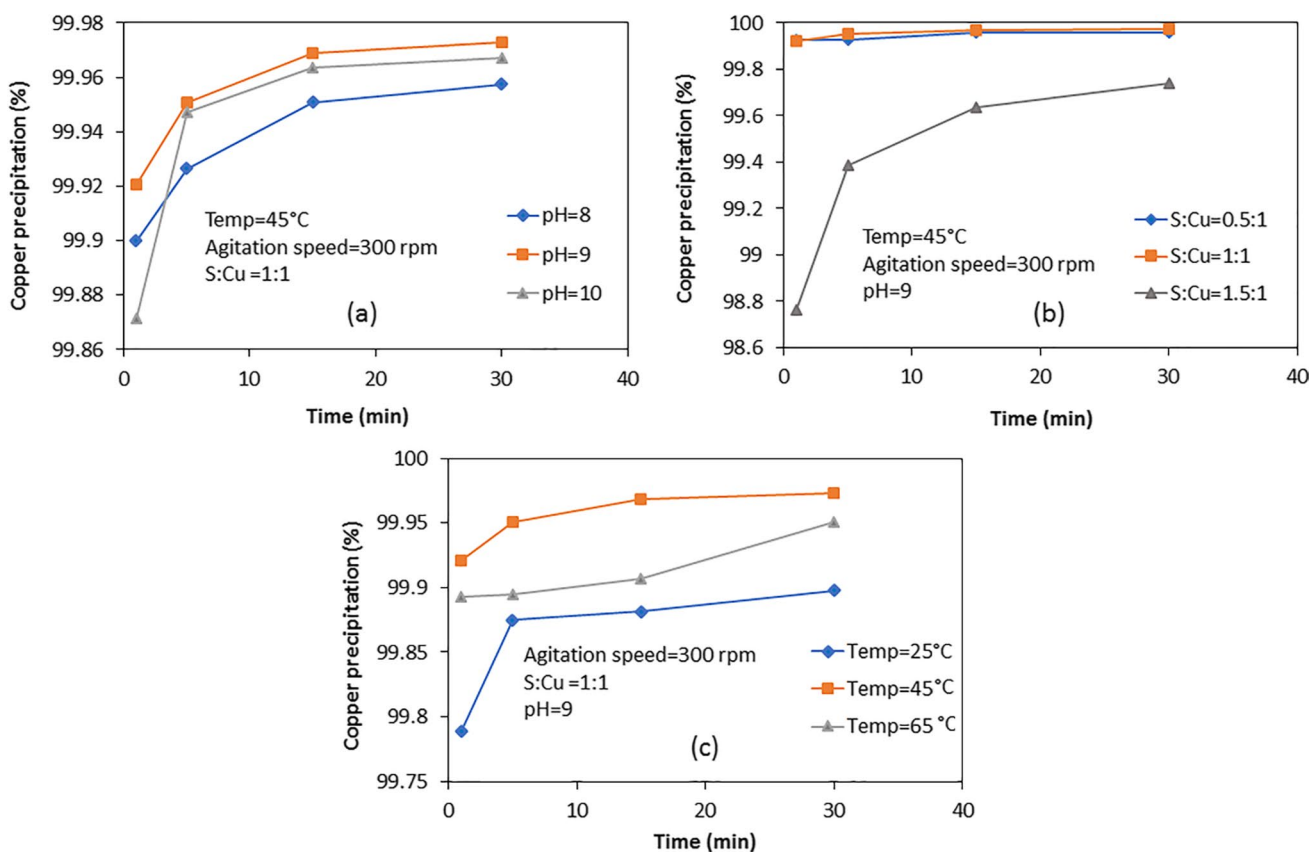
Fig. 14 Effect of **a** pH, **b** S:Cu ratio, and **c** temperature for precipitation process

are observed [9]. In electrochemically reversible electron-transfer processes with freely diffusing redox species, Randles−Sevcik equation (Eq. 12) describes how the peak current ip (A) increases linearly with the square root of the scan rate [13].

$$i_p = 0.446nFAC^0\left(\frac{nF\upsilon D_o}{RT}\right)^{1/2} \tag{12}$$

where i_p is peak current (A), n is the number of electrons transferred in a redox cycle, F is Faraday's constant (96,485.339 C/mol), R is the universal gas constant (8.31447 J.K^{-1}.mol^{-1}), T is the absolute temperature, A is
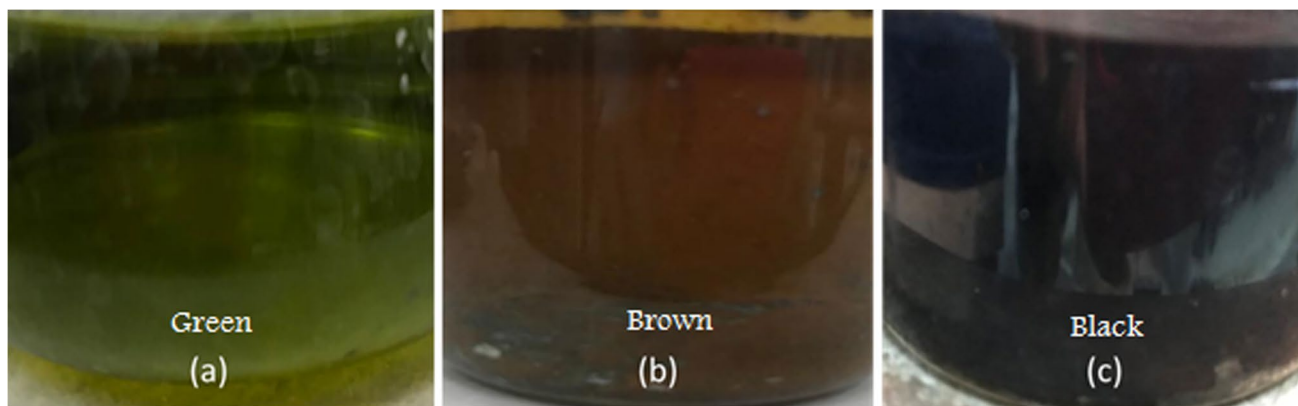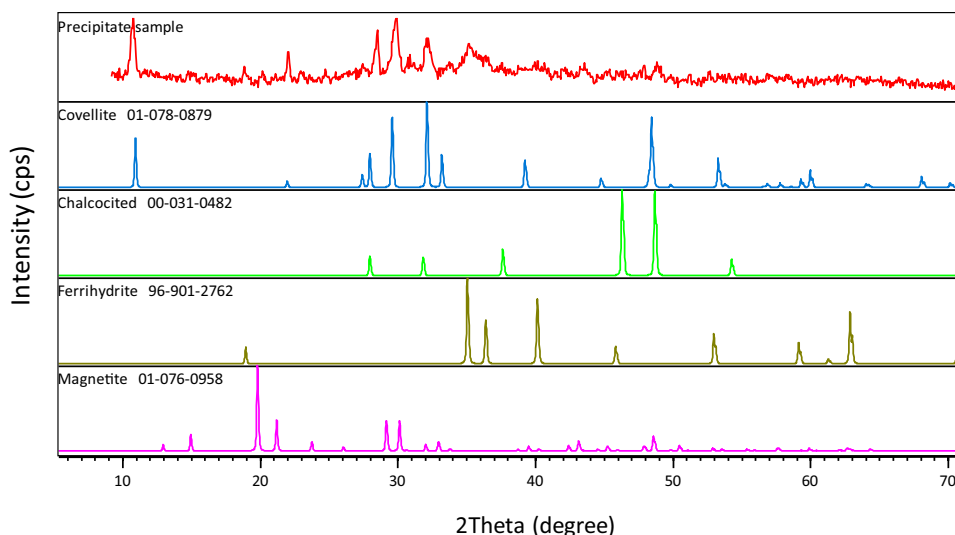

Fig. 15 Color of copper leaching solution **a** before precipitation, **b** after 1 min precipitation, and **c** after 30 min precipitation (S:Cu = 1, pH = 9, and 45 °C)

Fig. 16 XRD pattern of copper precipitate form copper leaching solution

the electrode surface area in working (cm^2), C is the molar concentration of redox-active species (mol/cm^3), D_o is the diffusion coefficient (cm^2/s), and v is the scan rate in V/s.

The linear dependence of the peak current on the square root of the scan rate is dependent on the diffusion. However, for molecules that adsorb on the electrode surface it will be dependent on the scan rate. In this area, the Randles − Sevcik equation (Eq. 13) can give indications as to whether an analyte is freely diffusing in solution [13].

$$i_p = \frac{n^2 F^2}{4RT} v A \Gamma^*$$ (13)

where i_p is peak current (A), n is the number of electrons transferred in a redox cycle, F is Faraday's constant (96,485.339 C/mol), R is the universal gas constant (8.31447 J.K^{-1}.mol^{-1}), T is the absolute temperature, A is the electrode surface area in working (cm^2), v is the scan rate in V/s, and Γ^* is the surface coverage of the absorbed species in mol/cm^2. As shown in Fig. 12a and b, in the diffusion-controlled process for leaching solution, the peak currents are linearly proportional to the square root of the scan rate. In surface-controlled (also known as an adsorption-controlled) process, as shown in Fig. 12c and d, the peak currents are linearly proportional to scan rate. Accordingly, for both redox peaks of cupper and ferric chloride, the diffusion-controlled process shows a higher R^2 (R-square) value than surface control.
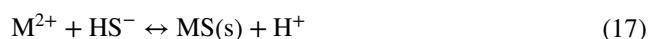
3.6 Kinetic Model

The rate of copper dissolution was controlled by both surface chemical reaction and diffusion through the interface of the unreacted core, as shown by the temperature dependence of copper leaching from the molybdenum concentrate (Fig. 7f). The model

curves showed a good linear fit to the kinetic data with regression coefficients, $R^2 > 0.95$. As shown in Fig. 13d and Table 6, the calculated intrinsic rate constants K were used to construct the Arrhenius plot. A good linear relationship ($R^2 > 0.90$) is observed in Fig. 13 which was employed to calculate the activation energy. The activation energy was achieved at 33.56 kJ/mol, which is typical for a process controlled by diffusion and chemical reactions. A fast dissolution rate for copper dissolution at the beginning of a time period verified the chemical reaction control and then diffusion through the product layer and interfacial transport for the dissolution mechanism.

3.7 Copper Precipitation Process

For an efficient sulfide precipitation process, Na$_2$S reacts with metal cations existing in an aqueous solution, according to the reaction mechanism described in Eqs. (14)–(17) [10].

$$H_2S \leftrightarrow HS^- + H^+$$ (14)

$$HS^- \leftrightarrow S^{2-} + H^+$$ (15)

$$M^{2+} + S^{2-} \leftrightarrow MS(s)$$ (16)

$$M^{2+} + HS^- \leftrightarrow MS(s) + H^+$$ (17)

For copper cations in leaching solution, the formation of CuS could be possible with a high pKsp value to form a stable precipitate [10]. To investigate the effect of pH on copper precipitation, the pH of solution was adjusted from 8 to 10 at 45 °C and S/Cu = 1. As shown in Fig. 14a, increasing the pH from 8 to 9 was sufficient for complete sulfide precipitation.

When the pH of the solution was raised to 10 in bisulfide solution, the presence of copper complexes in the form of CuS(HS)$_n^{-n}$

($n = 2$ and 3), as one possible explanation for a little increase in copper dissolution [26]. The results showed that the appropriate S/Cu ratio was equal to 1 to obtain the maximum precipitation rate (Fig. 14b). The reaction temperature is the other effective parameter that could affect the precipitation process. The precipitation reaction was carried out at different temperatures ranging from 25 to 65 °C. Figure 14c shows that the precipitation of copper was very fast. By increasing the temperature up to 45 °C, copper precipitation reached a maximum yield. After 45 °C, the precipitation rate did not change significantly.

The color of the initial precipitates was the other control parameter to find the ending time for precipitation of copper ions [26]. The changing color from green to brown represented the fast precipitation at the beginning of a time (1 min). A black color after 30 min showed the complete precipitation process for copper (Fig. 15).

As shown in Fig. 16, the XRD pattern of the precipitate obtained from the copper leaching solution indicates that the main components in this precipitate are copper sulfides such as covellite (CuS) and chalcocite (Cu_2S)). Iron in the precipitate is also present as ferrihydrite ($Fe_2O_3. 0.5\ H_2O$) and magnetite (Fe_3O_4).

4 Conclusion

Mineralogical studies indicated that the presence of copper sulfide minerals such as chalcopyrite in molybdenum concentrate as impurities required a further purification method to reach the standard level of copper content (< 0.5 wt.%) from an economic point of view.

The complete dissolution of copper was carried out by the hydrometallurgical method and selecting the optimum conditions (i.e., including $HCl = 1$ M, $FeCl_3 = 0.5$ M, $CuCl_2 = 0.05$ M, $CaCl_2 = 0.5$ M at 75 °C, 500 rpm, S:L = 1:10 during 60 min) to effectively reduce the copper content (< 0.1 wt.%) without the dissolution of molybdenum.

During the first minutes of the leaching process, surface chemical reactions represented the highest correlation coefficients, and then the interfacial transport and diffusion through the product layer controlled the reactions. Moreover, the calculated activation energy of 33.56 kJ/mol indicated that both chemical and diffusion reactions controlled the copper leaching process.

The effect of $CuCl_2$ on the leaching process of copper was greater than the other reagents. It was probably associated with its catalytic reaction to disrupt the passivating sulfur layer or other precipitation layers on the particle surface at the beginning of the process. Based on CV results, the presence of Cu^{2+} and Fe^{3+} as the oxidizing reagents could be very effective for copper dissolution. On the other hand, the presence of $CaCl_2$ and $FeCl_3$ in HCl media increased the concentration of chloride ions. Therefore, the formation of $CuCl_2^-$, $CuCl_3^{2-}$, and $CuCl_4^{3-}$ on the surface of sulfide minerals could

also prevent the formation of a passive layer by the increasing the Cu^{2+}/Cu^+ ratio and copper dissolution.

The precipitation of copper in the leaching solution could be effective in the convenient recovery of copper. Therefore, the recycling of the solution into the leaching operation could be possible. The optimum conditions to obtain the maximum precipitation rate were achieved at 45 °C, S/Cu ratio of 1, and pH = 9.

Data Availability We mentioned previously in the precipitation process for copper solution after removing from molybdenite concentrate, it is possible for copper to be precipate and separate from soultion, it is a way that would be applicale for copper to recycle from leaching solution and using into the copper extration unite.

Declarations

Conflict of interest The authors declare no competing interests.

References

1. Abdollahi H, Manafi Z, Shafaei Sied Z, Noaparast M, Manafi Moorkani N (2013) Removal of copper from molybdenite concentrate by mesophilic and extreme thermophilic microorganisms. Int J Min Sci Technol 23(6):827–834
2. Al-Harahsheh M, Kingman S, Al-Harahsheh A (2008) Ferric chloride leaching of chalcopyrite: synergetic effect of CuCl2. Hydrometallurgy 91(1–4):89–97
3. Bai S et al (2020) Ammonium chloride catalyze sulfidation mechanism of smithsonite surface: visual MINTEQ models. ToF-SIMS and DFT studies Minerals Engineering 146:106115
4. Bonan M, Demarthe J, Renon H, Baratin F (1981) Chalcopyrite leaching by CuCl2 in strong NaCl solutions. Metall Trans B 12(2):269–274
5. Cao Z-F, Zhong H, Qiu Z-H, Liu G-Y, Zhang W-X (2009) A novel technology for molybdenum extraction from molybdenite concentrate. Hydrometallurgy 99(1–2):2–6
6. Carvalho-Silva VH, Coutinho ND, Aquilanti V (2019) Temperature dependence of rate processes beyond Arrhenius and Eyring: activation and transitivity. Front Chem 7:380
7. Didyk-Mucha A, Pawlowska A, Sadowski Z (2016) Application of the shrinking core model for dissolution of serpentinite in an acid solution, E3S Web of Conferences. EDP Sciences, pp. 01035
8. Ebrahimzade H, Khayati GR, Schaffie M (2018) Leaching kinetics of valuable metals from waste Li-ion batteries using neural network approach. J Mater Cycles Waste Manage 20(4):2117–2129
9. Elgrishi N et al (2018) A practical beginner's guide to cyclic voltammetry. J Chem Educ 95(2):197–206
10. Estay H, Barros L, Troncoso E (2021) Metal sulfide precipitation: recent breakthroughs and future outlooks. Minerals 11(12):1385
11. Fu Y-F et al (2017) Pressure aqueous oxidation of molybdenite concentrate with oxygen. Hydrometallurgy 174:131–139
12. Fu Y-F et al (2018) Direct extraction of Mo(VI) from acidic leach solution of molybdenite ore by ion exchange resin: batch and column adsorption studies. Trans Nonferrous Metals Soc China 28(8):1660–1669

13. García-Miranda Ferrari A, Foster CW, Kelly PJ, Brownson DA, Banks CE (2018) Determination of the electrochemical area of screen-printed electrochemical sensing platforms. Biosensors 8(2):53

14. Gerhardt NI, Palant A, Petrova V, Tagirov R (2001) Solvent extraction of molybdenum (VI), tungsten (VI) and rhenium (VII) by diisodo-decylamine from leach liquors. Hydrometallurgy 60(1):1–5

15. Ghahremaninezhad A, Dixon D, Asselin E (2013) Electrochemical and XPS analysis of chalcopyrite (CuFeS2) dissolution in sulfuric acid solution. Electrochim Acta 87:97–112

16. Gill NS et al (1967) Tetrahalo complexes of dipositive metals in the first transition series. Inorg Synth 9:136–142

17. He S et al (2019) Kinetics of iron removal from Ti-extraction blast furnace slag by chlorination calcination. Open Chem 17(1):1146–1156

18. Hsieh M-T, Chen C-T, Whang T-J (2016) Triethanolamine-facil-itated one-step electrodeposition of CuAlSe2 thin films and the mechanistic studies utilizing cyclic voltammetry. J Electroanal Chem 762:73–79

19. Ikumapayi FK (2008) Purification of molybdenite concentrates

20. Itodo A, Eneji I, Mnenga B, Tseen M (2019) Chemical charac-terization and leaching kinetics of metals from iron ores. Acad J Chem 4(9):69–80

21. Kabtamu DM et al (2018) The effect of adding Bi 3+ on the per-formance of a newly developed iron–copper redox flow battery. RSC Adv 8(16):8537–8543

22. Kan S, Benzeşik K, Odabaş ÖC, Yücel O (2021) Investigation of molybdenite concentrate roasting in chamber and rotary furnaces. Mining, Metallurgy Exploration 38(3):1597–1608

23. Khalaghi B et al (2014) Electrochemical behaviour of dissolved iron chloride in KCl+ LiCl+ NaCl melt at 550°C. ECS Trans 64(4):301

24. Lasheen T, El-Ahmady M, Hassib H, Helal A (2015) Molybde-num metallurgy review: hydrometallurgical routes to recovery of molybdenum from ores and mineral raw materials. Miner Process Extr Metall Rev 36(3):145–173

25. Lessard JD, Shekhter LN (2014) Thermodynamic modeling of atmospheric hydrometallurgical removal of chalcopyrite from molybdenite concentrates. Hydrometallurgy 150:9–13

26. Lewis AE (2010) Review of metal sulphide precipitation. Hydro-metallurgy 104(2):222–234

27. Li Y, Kawashima N, Li J, Chandra A, Gerson AR (2013) A review of the structure, and fundamental mechanisms and kinetics of the leaching of chalcopyrite. Adv Coll Interface Sci 197:1–32

28. Lundström M, Aromaa J, Forsén O (2009) Redox potential character-istics of cupric chloride solutions. Hydrometallurgy 95(3–4):285–289

29. Lundström M, Aromaa J, Forsén O, Hyvärinen O, Barker MH (2007) Cathodic reactions of Cu2+ in cupric chloride solution. Hydrometallurgy 85(1):9–16

30. Malhotra D, Rowe RM, Bhasin AK (1986) Evaluation of collec-tors for molybdenite flotation. Mining, Metallurgy Exploration 3(3):184–186

31. Manukyan K, Davtyan D, Bossert J, Kharatyan S (2011) Direct reduction of ammonium molybdate to elemental molybdenum by combustion reaction. Chem Eng J 168(2):925–930

32. Nadimi H, Sarpoolaky H, Soltanieh M (2021) Formation reac-tion kinetics of nanocrystalline TiC via molten LiCl–KCl apply-ing shrinking core model. Ceram Int 47(9):12859–12869

33. Nazim M, Ameen S, Akhtar MS, Shin H-S (2019) Electrochemical detection of chloride ions by copper (II) complex with mixed ligand of oxindole derivative and dithiocarbamates moiety. Appl Sci 9(7):1358

34. Nicol M, Miki H, Zhang S (2017) The anodic behaviour of chal-copyrite in chloride solutions: Voltammetry. Hydrometallurgy 171:198–205

35. Nicol MJ, Tjandrawan V, Zhang S (2016) Cathodic reduction of iron (III) and copper (II) on various sulfide minerals in chloride solutions. Hydrometallurgy 166:113–122

36. Nozari I, Azizi A (2020) Experimental and kinetic modeling inves-tigation of copper dissolution process from an Iranian mixed oxide/sulfide copper ore. J Sustain Metallurgy 6(3):437–450

37. Ojeda M, Rivarola J, Quiroga O (2002) Study on chlorination of molybdenum trioxide mixed with carbon black. Miner Eng 15(8):585–591

38. Padilla R, Letelier H, Ruiz MC (2013a) Copper removal from molybdenite by sulfidation-leaching process, materials processing fundamentals. Springer, pp. 217–223

39. Padilla R, Letelier H, Ruiz MC (2013) Kinetics of copper dissolu-tion in the purification of molybdenite concentrates by sulfidation and leaching. Hydrometallurgy 137:78–83

40. Pestryak I, Morozov V, Baatarhuu J (2013) Improvement of cop-per–molybdenum ore beneficiation by a combined flotation and biohydrometallurgy method. Int J Min Sci Technol 23(1):41–46

41. Prasad PM, Balasubramanian K, Mukhopadyay R (2007) Separa-tion chemistry in the refining of an off-grade molybdenite concen-trate by leaching with an acid mix. Mining, Metallurgy Explora-tion 24(2):97–104

42. Rahimi Borujerdi P, Shotorban B, Mahalingam S, Weise DR (2019) Modeling of water evaporation from a shrinking moist biomass slab subject to heating: Arrhenius approach versus equi-librium approach. Int J Heat Mass Transf 145:118672

43. Rasulova S, Guro V, Safarov E, Adinaev X (2020) Metals recovery from molybdenite concentrate by electrooxidation and leaching, IOP Conference Series: Materials Science and Engineering. IOP Publishing, pp. 012076

44. Rukini A, Rhamdhani MA, Brooks GA, Van den Bulck A (2022) Metals production and metal oxides reduction using hydrogen: a review. J Sustain Metallurgy 8(1):1–24

45. Schueler TA, de Aguiar PF, Vera YM, Goldmann D (2021) Leaching of Cu, Zn, and Pb from sulfidic tailings under the use of sulfuric acid and chloride solutions. J Sustain Metallurgy 7(4):1523–1536

46. Sun X, Yuan W, Jin K, Zhang Y (2021) Control of the redox potential by microcontroller technology: researching the leaching of chalcopyrite. Minerals 11(4):382

47 Timoshevsky A, Yemel'Kin V, Pozdnyakov B, Zasypkin I (2006) Plasma-thermal decomposition of molybdenite, equipment and experiment. Thermophys Aeromechanics 13(4):609–614

48. Velásquez-Yévenes L, Nicol M, Miki H (2010) The dissolution of chalcopyrite in chloride solutions: part 1. Effect Solution Potential Hydrometallurgy 103(1–4):108–113

49. Vračar RŽ, Parezanović IS, Cerović KP (2000) Leaching of copper (I) sulfide in calcium chloride solution. Hydrometallurgy 58(3):261–267

50. Wilkomirsky I, Becker J, Parada F (2022) Molybdenite concen-trate purification by a continuous sulfation-leaching process. Min-ing, Metallurgy & Exploration

51. Yin Z et al (2016) Investigation into the flotation response of refractory molybdenum ore to depressant mixtures: a case study. Int J Min Sci Technol 26(6):1089–1094

52. Yoo K et al (2010) Effect of chloride ions on leaching rate of chalcopyrite. Miner Eng 23(6):471–477

53. Youcai L, Hong Z, Zhanfang C (2011) Molybdenum removal from copper ore concentrate by sodium hypochlorite leaching. Mining Sci Technol (China) 21(1):61–64